Electrochemical impedance spectroscopy study of lithium–sulfur batteries: Useful technique to reveal the Li/S electrochemical mechanism

Sylwia Waluś, Céline Barchasz, Renaud Bouchet, F. Alloin

Electrochemical Impedance Spectroscopy study of Lithium–Sulfur batteries: Useful technique to reveal the Li/S electrochemical mechanism.

Sylwia Waluś[1,2], Céline Barchasz[2], Renaud Bouchet[1*], Fannie Alloin[1,3*]

[1]Univ. Grenoble Alpes, Univ. Savoie Mont Blanc, CNRS, Grenoble INP, LEPMI, 38 000 Grenoble, France

[2] Univ. Grenoble Alpes, CEA, LITEN, DEHT, STB, F-38054 Grenoble

[3]Réseau sur le Stockage Electrochimique de l'Energie (RS2E), CNRS, FR3459, 80039 Amiens Cedex, France

*Corresponding author: +33 4 76 82 65 61 fannie.alloin@lepmi.grenoble-inp.fr; Renaud.bouchet@lepmi.grenoble-inp.fr

ABSTRACT

Electrochemical impedance spectroscopy (EIS) study was done in order to go deeper into the electrochemical processes of Li/S battery in a common CR2032 coin-type cell. In order to separate the contributions of each electrode (i. e. lithium negative electrode and sulfur composite positive electrode), impedance measurements on symmetrical cells consisting of two previously cycled electrodes was used. This methodology enables to propose an overall interpretation of the different electrochemical phenomena present during cycling. Low temperature tests were also applied, which brought fruitful information concerning the kinetics of the reactions and allowed to confirm the chemical-physical interpretations performed on the cell cycled at 25°C.

KEYWORDS:

Lithium-sulfur battery, electrochemical impedance spectroscopy, electrochemistry, equivalent electrical circuit

Introduction

Lithium/Sulfur (Li/S) technology is expected to offer 2-3 times the energy density of best performing Li-ion batteries, with reduced costs. Due to its high theoretical performances, Li/S batteries have become a 'hot topic' within the battery research and industry. However, many limitations are known for this system, which hinder the complete technological transfer to the

commercial market. EIS is a very powerful technique that enables the separation of electrical processes occurring in an electrochemical cell according to their specific relaxation frequencies. Therefore, main electrochemical behaviors and their evolution can be elucidated from the EIS response. The literature reports on many examples where EIS was applied to Li/S cells for the following purposes: characterization of the electrolyte properties [1], investigation of SEI (solid electrolyte interphase) at the lithium interface [2], evaluation of electrode electric response in regard to their composition [3], analysis of the capacity fading [4,5] or more generally to study the electrochemical mechanism [2,6–13] upon cycling. Different cell configurations have been reported, two-electrode full cells, symmetric cells, three-electrode and four-electrode cells. Three-electrode cell configuration needs a reference electrode that permits to obtain separately the response of the anode and cathode electrodes. However, the electrochemical asymmetry between both electrodes causes distortion of the EIS spectra [14], which can induce misinterpretations. To partially overcome this issue, X. Qiu et al.[13] performed the study of the discharge/charge process in a glassy three-electrode cell, in order to limit the perturbation induced by the presence of the reference electrode. Nevertheless, the large amount of electrolyte makes this cell not very representative of a real system. The chosen design of a four-electrode cell was recently proposed in a common CR2032 coin-type cell [6]. The design chosen was Li/S-CP/S-CP/Li where S-CP is a carbon paper electrode with sulfur deposited through melt-diffusion and each electrode was separated by a separator swollen by liquid electrolyte. Even if the expected evolutions upon cycling were obtained, the complexity of the cell induces large resistance values. In addition, the response of the S-CP electrodes was present in the impedance spectra when the Li/Li symmetric cell was investigated. The two-electrode full cell is likely to be more representative of a real system. However, the overall impedance response makes it difficult to distinguish the specific contributions from both electrodes and it is challenging to correlate it with the underlying physical-chemical processes. Hence, in order to determine univocally the contribution of each electrode, one powerful and useful technique is EIS measured on symmetrical cells consisting of two pre-cycled electrodes of the same type assembled into a coin cell, as previously reported in the literature [1,10,11].

In this paper, we propose to use EIS technique in order to reveal the electrochemical processes of Li/S battery in a common CR2032 coin-type cell, and to propose an overall interpretation of the different electrochemical phenomena present during cycling. Low temperature tests were also applied, which brought fruitful information concerning the kinetics of the reactions and allowed to confirm the physico-chemical interpretations performed on the cell cycled at 25 °C.

Experimental section

1. Materials, electrodes formulation, coin cell assembly

Sulfur (-325 mesh, Alfa Aesar), Carbon black (SuperP Li®, Timcal) and PVdF 5130 (Solvay) were dried. The electrode composition was 80/10/10 wt% (S/SuperP®/PVdF 5130). After homogenization, the ink was coated using doctor-blade technique onto a non-woven carbon (NwC) paper (H2315®, 210 µm thick, from Freudenberg) as a current collector. Sulfur loading was close to 4.3 mg_{sulfur} cm^{-2}. Effective thickness of a final sulfur electrode was about 270 ± 10 µm. More details concerning preparation and properties of such prepared sulfur electrode can be found in our previous publication [15]. Electrodes were dried at 55 °C during 24 h, cut into Ø 14 mm disks, dried at room temperature under vacuum, and finally entered in an argon-filled glove box for coin cells fabrication. A standard liquid electrolyte composition was chosen, composed of 1M lithium bis(trifluoromethane sulfonyl)imide salt (LiTFSI, 99.95 %, Solvay), in a mixture of tetraethylene glycol dimethyl ether (TEGDME, 99 %, stored on molecular sieves, Aldrich) and 1,3-dioxolane (DIOX, anhydrous, 99.8 %, stored on molecular sieves, Aldrich) in 1/1 volume ratio. Lithium nitrate (0.1 M $LiNO_3$, Aldrich) was used as an additive commonly known from its beneficial effect against polysulfide shuttle [16].
CR2032 two-electrode coin cells were prepared by stacking positive electrode disk, layer of Celgard®2400 separator with additional layer of thick (240 µm, Viledon®, from Freudenberg) polyolefin non-woven felt which serves as an electrolyte reservoir. 100 µL of electrolyte was poured on the separators and then covered by a disk of metallic lithium (Rockwood Lithium; 135 µm; Ø 16 mm) the negative electrode.
Symmetric coin cells' preparation was identical as described above, except that two cathodes ($S_8||S_8$) or two anodes (Li||Li) were assembled into one coin cell. Two types of symmetric cells were made, where either fresh or pre-cycled electrodes were used. More details on experimental procedure about pre-cycled symmetric coin cell assemblies are provided in Figure S1.

2. Electrochemical measurements

EIS tests were performed on Bio-Logic® VMP3 multichannel potentiostat equipped with impedance modules. Each spectrum was measured in the frequency range of 1 MHz to 10 mHz, with an excitation potential of 10 mV and 13 points per. Obtained results were then fitted using ZView software (Scribner Associates Inc.). ~~*In situ*~~ EIS was recorded on the Li/S two-electrode coin cells galvanostatically cycled at C/20 rate, in the potential window of 3.0 V - 1.5V. The

potenstiostatic EIS spectra were registered every 1 h, after 15 min of relaxation applied prior to the measurement. C/20 cycling regime was selected as a trade-off between ensuring that all reactions of interest took place in a reasonable amount of time.

Results and discussion

As mentioned previously, in order to clearly separate the two electrode contributions in a complete Li/S coin cell, supportive data were obtained from measuring EIS of symmetric coin cells (Li||Li, S_8||S_8), either fresh or previously cycled to a chosen SoC% (Figure S1).

1. OCV response of the cell

1.1 Initial EIS response

Characteristic Nyquist plot of a fresh two-electrode Li/S cell is shown in Figure 1. In the first approach, Nyquist plot can be divided in three main regions. The high frequency (HF) region can be attributed to the ohmic contributions of the cell (ionic migration in the electrolyte, all the electrical connections (coin cells casing, cables, sample holder). The straight line almost vertical in the low frequency region (LF) is generally attributed to the blocking electronic charge transfer of the system *vs.* electrochemical reaction. A CPE is proposed for modeling this part of the spectra [17]. However, the origin of the depressed loop in the middle frequency (MF) region is still controversial and different interpretations can be found in the literature [4,18]. In order to attribute, without any ambiguity, the middle frequency (MF) loop, symmetric coin cells were prepared and characterized.

Figure 2a shows Nyquist plots of fresh symmetric cells composed of two similar electrodes (Li||Li, S_8||S_8), which are compared with the initial spectrum of the complete Li/S cell.

Firstly, the S_8||S_8 response is mainly dominated by the blocking behavior of the insulant sulfur, which gives the low frequency contribution in the complete Li/S cell. It exhibits a very small semi-circle (~2 Ω) at a quite high frequency, of ~9 kHz. In accordance with literature [10,19], this response is associated with the existence of polarization through the composite electrode due to bad electronic contacts between the sulfur particles bound together by the carbon particles and the binder. In any case, the contribution of the positive electrode to the MF loop is marginal and cannot be easily distinguished in the spectrum of the Li/S. On the other side, the characteristic frequency of the MF semicircles in complete (Li/S) and symmetric Li||Li cells are almost identical, with the same amplitude. Therefore, the loop in the MF range can be

attributed univocally to the lithium negative electrode, with a main contribution coming from the passivation layer on the lithium surface [20–22].

One could also notice the presence of a LF loop distorted in the lowest frequencies for the symmetric Li||Li cell (red dotted line in Figure 2a). The literature often attributes this contribution to the electronic charge transfer occurring on the negative electrode in parallel with the double layer capacitance [21]. In our case however, the capacitance associated to this semicircle, is close to $\sim 2 \cdot 10^{-3}$ F.cm^{-2} which is not coherent with the double layer capacitance known to be in the range of 1-50 μF.cm^{-2} for flat metallic electrodes [23]. The LF loop could rather originate from a diffusion processes through passivation layer(s) on Li surface, *i.e.* thin compact SEI sublayer and porous thicker SEI layer and, at lower frequencies (the tails of the loop at frequencies <10 mHz), from the diffusion process into the electrolyte through the porous separator [22]. This observation is in a good agreement with the report of Woo *et al.* [23] who studied symmetrical Li||Li cell degradation, with the study of J. Fang *et al.* in the four-electrode cell configuration [6], and with the transmission line model used for the investigation of Li dendritic growth in lithium electrode [22].

To confirm the validity of the symmetric cell approach, experimental data of the complete cell (Li/S) were compared with the calculated one (Figure 2b; experimental details in Figure S1), according to the equation: $Z_{Li\text{-}S}(\omega) = ½\, Z_{Li\text{-}Li}(\omega) + ½\, Z_{S\text{-}S}(\omega)$, where ω is the pulsation in rad.s^{-1}. Both graphs are superimposed in the whole frequency range, proving the pertinence of the symmetric cell approach used to separate the two electrode contributions of the complete cell. In addition, the frequency distribution at the feet of the LF strait line can be attributed to the diffusion processes trough the SEI occurring at the negative electrode.

1.2 Evolution with time: Self-discharge

Li/S coin cell was stored for 250 h at a temperature of 25± 0,1 °C and OCV was monitored. EIS spectra was recorded every 30 min. Figure 3 shows the evolution of OCV and selected EIS spectra. It can be seen that the vertical line in the low frequency region is slowly losing its blocking character with time. The reason for that is attributed to sulfur dissolution in the electrolyte [24] which then diffuses to the negative electrode side and gets reduced to high-order polysulfides, inducing self-discharge with the potential stabilization at 2.45 V *vs* Li. Lithium polysulfides are electrochemically active, which explain the complete disappearance of blocking/capacitive behavior relatively quickly. In addition, the MF semicircle which was

previously attributed to the passivation layer on the lithium surface, progressively increases, together with the characteristic frequency shifting into lower value (*i.e.* 864 Hz at the initial state; 266 Hz after 250 h of storage).

Indeed, very similar behavior is found when symmetric Li||Li cell is left for storage. Almost identical trend of MF semicircle evolution is observed (Figure 3d). This suggests that the increase of the resistance of that MF loop is due to the increase of the passivation layer on the lithium metal, caused by decomposition of the electrolyte when in contact with Li [11,22].

2 Li/S cell upon cycling

2.1 Nyquist plot parameters

Two similar Li/S coin cells were cycled at C/20. High capacity of 1100 mAh g^{-1} was achieved during the initial discharge, followed by stabilized value at around 800 mAh g^{-1} (Figure S2). During the initial discharge and charge, the cell was stopped every 1 h and relaxed for 15 min to reach the equilibrium potential, before EIS was measured. Figure 4 shows the evolution of the Nyquist plot obtained along the initial cycle. Voltage profile of the first discharge and charge, when under load and during relaxation, is shown in Figure S3.

It can be clearly seen that Nyquist plot significantly varies as a function of SoC%. If correlating the spectra recorded at different SoC% with the experimental discharge voltage profile, following statements can be concluded:

- Along the upper discharge plateau and the region between the two plateaus (plots 1-5 in Figure 4), no large evolution is observed. Instead, a small decrease of the MF semicircle is visible and the appearance of a little LF semicircle is observed.
- Along the lower discharge plateau, a strong decrease of the MF semicircle is observed. In addition, a significant increase of LF semicircle towards the end of lower discharge plateau can be seen, reaching its maximum at the very end of discharge (plot 16 in Figure 4).
- During charge, the MF loop stays almost constant whereas, a reversible decrease of the LF semicircle is observed, up to the formation of S_8.

To avoid ambiguity in the phenomena observed, similarly to the information-rich approach performed at OCV (section 1.1.), symmetric cells were prepared from pre-cycled electrodes, discharged down to 2.1 V *vs* Li (Figure S1), then disassembled in glove box to get the two Li and positive (PS) electrodes that were reassembled in symmetric cells. Nyquist plots of the

complete Li/S cell measured at 2.1 V together with the EIS data of symmetric cells are shown in Figure S4a.

At 2.1 V *vs* Li, the $S_8||S_8$ symmetric cell demonstrates two small semicircles. The one at high frequency (~10 kHz, ~1 Ω) has already been attributed to the intrinsic bulk response of the positive electrode, while the larger one (~8 Ω) with frequency of 37 Hz is attributed to the electronic charge transfer reaction due to soluble polysulfides electrochemical reaction. Similar to what was observed in section 1.1 (Figure 2), it appears that at 2.1 V *vs* Li, lithium electrode is largely contributing to the global response of Li/S cell, with a principal contribution due to its passivation layer at a characteristic frequency identical to the complete Li/S cell (~1 kHz). Finally, the low frequency diffusion process is also partially related to the negative electrode and the diffusion of Li^+ through the passivation layer(s) as discussed previously, but also in the porous sulfur electrode and the electrolyte (soluble polysulfides S_n^{2-} and Li^+), however these correlated different diffusion processes are rather difficult to distinguish. The in-depth study of the lithium electrode with and without polysulfides is outside the scope of this article and it is very well explained in the work of S. Drvaric Talian et al.[22,25].

The approach of symmetric cells was again validated by comparing the 'experimental' and 'calculated' spectra (details of calculations are in SI; Figure S4b). Again a good match between both curves was obtained, which makes our attribution univocal.

To summarize, these studies on symmetric cells allow us (i) to explain the origin of each Nyquist plot component in a full Li/S cell and (ii) to propose an equivalent electrical circuit (Figure 5), which can be used for fitting the data at different SoCs%. This model is composed of the following blocks connected in series:

- **R_{el} -** attributed mainly to the electrolyte and electrical connection resistances
- **R_{NwC}//CPE_{NwC} -** corresponds to the positive electrode bulk contribution associated with its microstructure
- **R_{Li}//CPE_{Li}** – mainly attributed to the lithium/electrolyte interphase (SEI)
- **R_{PS}//CPE_{PS}** - corresponds to the charge transfer of polysulfides species on positive electrode
- **CPE_{diff} -** corresponds to the diffusion processes through the electrolyte, the passivation layer on lithium surface and inside the porous positive electrode

2.2. Evolution of the different parameters during the first discharge and charge

Figure 6 shows the evolution of resistance values, previously attributed to different phenomena *i.e.* electrolyte resistance (R_{el}), lithium/electrolyte interphase (R_{Li}), polysulfides/carbon

electronic charge transfer resistance (R_{PS}) and bulk response of NwC collector (R_{NwC}), together with corresponding voltage profile.

HF response

The changes in the high frequency (HF) region are mainly associated with the electrolyte resistance (R_{el}) evolution related to the concentration and composition of soluble polysulfide species in the electrolyte. The electrolyte resistance evolution recorded during initial cycle is similar to the literature data [9,18,26]. The resistance increases at the beginning of discharge, mainly due to the viscosity increase associated with the PSs concentration increase and the formation of shorter PSs. Indeed, the 0.1 M and 1 M of equivalent Li_2S_4 solutions exhibit a viscosity of 2.10^{-2} Pas and 8.10^{-2} Pas respectively, whereas the 0.1 M equivalent Li_2S_8 and Li_2S_4 exhibit a viscosity of 5.10^{-3} Pas and 2.10^{-2} Pas respectively. The resistance reaches a maximum when the formation of solid Li_2S starts to occur [27], resulting in soluble species consumption and the decrease of electrolyte viscosity and thus resistance of the electrolyte.

During charge, a reversible behavior is observed, linked to the progressive oxidation of Li_2S accompanied with the formation of low-to-mid order PSs, which in turn causes the increase of viscosity. The maximum point is in accordance with the moment of complete Li_2S disappearance, shown by *operando* XRD [27,28]. Afterwards, formation of solid sulfur requires consumption of soluble high order PS species (S_6^{2-}, S_8^{2-}), thus the electrolyte resistance decreases. The difference in the position of the resistance maximum between the charge and discharge is directly correlated to Li_2S formation/re-oxidation hysteresis pointed out by *operando* XRD measurement [27,28] and in accordance with the literature data obtained in four-electrode cell design [6].

The electrolyte resistance never comes back to the initial value and remains slightly higher (grey dashed line in Figure 6a). Even at the end of first discharge and charge, some polysulfides are still present in the electrolyte, showing an incomplete reversibility of the system, which underline the role of the electrolyte as a polysulfides' reservoir.

When comparing the evolution of maximum resistance value with the capacity retention during further cycles, a very good correlation is observed: *i.e.* a decrease of the maximum electrolyte resistance along with capacity fading, except for the initial cycle (Figure 7), which reflects the loss of soluble PSs, and consequently of active material. Such continuous decrease of the electrolyte resistance could be related with the fact that low amount of polysulfides is fixed in the electrolyte at each cycle when cycle number increases. This progressive loss of active material could be due to the irreversible precipitation of Li_2S or Li_2S/Li_2S_2 far from the

electronic network, which then become inaccessible during next cycles. After few cycles, the electrolyte resistances at the end of both charge and discharge are similar and remain constant upon cycling, which indicates that there is no accumulation of insoluble and non-connected PS species in the battery. That is in a good correlation with our hypothesis about the presence of precipitate species inside the electrolyte.

MF response

The semicircle (~1-2 Ω, at ~6-9 kHz) at the initial state of Li/S cells attributed to the bulk of positive electrode is masked by the Li negative electrode response (Figures 4 and 6b). Therefore, along the whole cycle and successive cycles, a relatively constant contribution of R_{NwC} is present, in accordance with a mechanically stable electronic network when using NwC current collector [15]. Regarding the porous structure of sulfur electrode, the impedance responses presented in the literature could be somehow different, with a quasi-diffusion feature observed at HF, which is ascribed to the porous character of the electrode assuming an infinite electronic conduction [29–31]. Nevertheless, the very small impedance response of the sulfur electrode obtained in our work does not allow us to extract properly this contribution. However, that observation reported in [30-32] should be taken into account for electrodes having a more significant impedance response. Thus, the evolution of the MF semicircle upon cycling is mainly associated with the modification of the passivation layer properties on the metallic lithium. Regarding its evolution, the resistance continuously decreases whereas the specific relaxation time increases during lithium oxidation along discharge. Such resistance evolution was already reported in the Li-ion cell studies [32]. The shift to higher values of the characteristic frequency of the MF loop (1 kHz to 8 kHz) can be associated with the chemical evolution of the passivation layer. In addition, these evolutions of the MF loop (characteristic frequency and resistance values) are very similar to the one obtained using symmetric Li/Li coin-cell with dissolved polysulfides in the electrolyte (0.25 M equivalent Li_2S_6), which is not the case without PSs additives (Figure S5). These results show the strong impact of the PSs on the lithium passivation layer, which most likely change its composition and thickness, leading to an overall less resistive layer.

During the following charge, the resistance of the lithium electrode remains very small, and slightly increases by the end of charge. This evolution may be related to the passivation layer evolution due to high order PSs associated with an increase of the layer's thickness. Regarding the evolution of the Li interphase response during cycling, it can be seen that the resistance

stays very small (~4 Ω) and stable. After the 1st cycle, the surface of Li is stabilized. A very similar situation is observed for the capacitance values.

LF response

The evolution of the LF contribution, previously attributed to the electronic charge transfer reaction of the polysulfide species (R_{PS}/CPE_{PS}), is shown in figure 6c as along the discharge and the charge. At the beginning of the discharge, the LF loop appears as a small loop at a frequency of ~37 Hz after the end of the first discharge plateau (point 3 in Figure 4). This contribution is dominated by the large response of the SEI and diffusion processes. Between the two plateaus (2.3 V – 2.1 V *vs* Li^+/Li), although, the polysulfides concentration is progressively increasing (see R_{el} evolution in Figure 6a), the charge transfer resistance stays small, suggesting a fast kinetics ($S_8 + 2Li^+ + 2e^- \Rightarrow Li_2S_8$, and $Li_2S_8 + 2Li^+ + 2e^- \Rightarrow 2\ Li_2S_4$). On the 2nd plateau (2.1 V vs Li), the semicircle starts to be clearly identifiable (point 7 in Figure 4) and exponentially diverges after the middle of the lower plateau (point 10 in Figure 4). In the same time, the relaxation frequency decreases (~2 Hz). This evolution is concomitant with a strong increase of the transport limitation, because the low frequency diffusional contributions increase as well. This divergence can be ascribed to the formation of an insulating layer on the surface of the electronic network in the positive, composed of precipitated Li_2S, which progressively blocks the electroactive surface, and thus limits the electronic charge transfer reaction. It shows that this blocking behavior drives the end of discharge with a brutal increase of polarization while full capacity was not obtained. This strong evolution of the charge transfer reaction resistance at the end of the discharge was widely reported in the literature [4,6,13]. The evolution obtained herein is in agreement with *operando* XRD observations [27], which show that the formation of insoluble and insulating Li_2S starts at the beginning of the lower discharge plateau with a continuous increase of Li_2S amount towards the end. As the electrochemical reaction kinetics is proportional to the electroactive surface, the reaction becomes really slow only when a large part of the electroactive surface is covered by an insulating layer of Li_2S, which seems to occur at the end of the second plateau.

During the subsequent charge, in a reversible manner, the charge transfer resistance drops rapidly. This explains the overpotential peak at the beginning of the charge, which is attributed to the slow kinetics of the Li_2S oxidation [17]. Indeed, after the polarization barrier is overcome, the charge transfer resistance decreases very rapidly but it is still observed until the beginning of the higher plateau (point 25 in Figure 4). It seems that Li_2S remains until the beginning of the upper charge plateau, which is in agreement with XRD observations concerning the moment of complete Li_2S consumption, *i.e.* up to the formation of sulfur [26].

3 Effect of temperature

3.1 Cycling voltage profiles

Discharge profiles of the Li/S cell cycled at different temperatures (Figure 8) clearly show that the upper discharge plateau is weakly affected by the temperature lowering, because it corresponds to the fast kinetics processes. When the temperature decreases, two plateaus started to appear progressively in the first part of the discharge curve, since both the electrochemical reactions and the equilibriums in between soluble polysulfides are slowed down. Most likely the nature and composition of polysulfides mixtures are much more defined when the temperature decreases, which enables the appearance of an intermediate small plateau. On the contrary, the lower discharge plateau corresponding to the Li_2S formation is very dependent on the temperature- strong increase of polarization and capacity lowering, since it is related with the formation of a thin insulator layer on the electrode surface, which induces slower kinetics of the reaction. At -40°C, the lower discharge plateau disappears, because of a huge polarization, which may be due to the precipitation of shorter polysulfides (S_4^{2-}, S_2^{2-}), leading to the blocking of the electrode electroactive surface.

3.2 Impedance parameter evolution

In-situ impedance spectroscopy was performed on the Li/S cell at different temperatures. The evolution of the electrolyte resistance shows the same trend as previously discussed for 25 °C, with the maxima obtained for the same state of charge regardless the temperature where the Li/S has been cycled (Figure 9a). Thus, the appearance and disappearance of insoluble polysulfides seem to be independent on the temperature. In particular, the appearance of insoluble Li_2S at the beginning of the second plateau is preserved at different the temperatures as well. When plotting the maximum resistance values recorded during discharge and charge

as a function of temperature (1000/T), classical thermally activated evolution is observed (Figure 9b), suggesting that the main parameter is the increase in viscosity with temperature, without significant evolution of the polysulfides concentration.

As discussed previously, at the end of discharge the electrolyte resistance never comes back to the initial value. However, at 25 °C the difference is low, whereas at -30 °C, the resistance at the end of discharge is much higher than the initial value *i.e.* 70 Ω instead of 35 Ω. Therefore, higher amount of soluble polysulfides is still present in the electrolyte at the end of discharge when the potential drops abruptly, which results in higher resistance value. On the contrary, the resistance at the end of charge is just marginally higher than the value observed at the initial step for the all temperatures, indicating a good reversibility of the oxidation of soluble polysulfides into sulfur even at -30 °C.

At the end of discharge, the loop at low frequency (Figure 10a) associated with the charge transfer resistance at the sulfur electrode, R_{PS}/CPE_{PS}, stays very similar when the temperature is decreased even if the SoCs% obtained at the end of discharge are really different. According to our previous results, the end of discharge is due to the exponential divergence of R_{PS} which induces a brutal increase of the polarization, i.e. the potential signature of the end of the discharge. Therefore, these results suggest that the blocking of the reduction to low order PSs (Li_2S_4, Li_2S_2, Li_2S) due to the formation of insulator passive layer onto the electroactive surface of the positive electrode is reached sooner when the temperature is decreased.

Finally, at the end of charge, the resistance of the electronic charge transfer, corresponding to the formation of sulfur, with the same SoC% (i.e. 100%) is continuously increasing while temperature decreases (Figure 10b), which demonstrates the strong thermal activation of this process. Indeed, the activation energy of the process is equal to 0.67 eV (Figure S6). Such high activation energy could be related to an electrochemical process coupled with a chemical process involving sulfur crystallization.

Conclusion

The approach combining EIS measurements on a classical two-electrode and symmetric coin cells enabled to carry out *in situ* impedance measurements on Li/S battery in a relevant and simple way. Our investigation permitted to propose a simple equivalent circuit valid all along the cycling. The circuit includes the electrolyte resistance response at high frequency (HF) region, followed by three R/CPE elements connected in series between medium frequency (MF) to low frequency (LF) regions, associated with i) the positive electrode bulk contribution, ii) the SEI contribution on the lithium surface, and iii) the charge transfer reaction of polysulfides

at the positive electroactive surface, respectively. Finally, at the lowest frequency, the response was related to the diffusion processes in the overall cell. The capacity retention upon cycling matches perfectly with the electrolyte resistance evolution, indicating progressive loss of active material during cycling. The decrease of temperature seems, at the beginning of the discharge, to lead to a better separation of the high order soluble polysulfides reduction with the appearance of a new small plateau around 2-2.1 V *vs* Li^+/Li, associated with a good reversibility and a fast kinetics. On the contrary, at higher State of Discharge, the precipitation of low order PSs limits the reachable capacity by blocking the electroactive surface. This reaction is not reversible and presents a high activation energy value, which strongly limits the capacity obtained on the lowest plateau when the temperature decreases.

Acknowledgements

The authors would like to acknowledge the CEA-INSTN and DGA (France) for PhD funding awarded to Sylwia Waluś. This research was performed in the framework of "Réseau sur le Stockage Electrochimique de l'Energie" (RS2E).

References

[1] S. Drvarič Talian, J. Moškon, R. Dominko, M. Gaberšček, Reactivity and Diffusivity of Li Polysulfides: A Fundamental Study Using Impedance Spectroscopy, ACS Appl. Mater. Interfaces. 9 (2017) 29760–29770. https://doi.org/10.1021/acsami.7b08317.

[2] L. Yuan, X. Qiu, L. Chen, W. Zhu, New insight into the discharge process of sulfur cathode by electrochemical impedance spectroscopy, J. Power Sources. 189 (2009) 127–132. https://doi.org/10.1016/j.jpowsour.2008.10.033.

[3] H. Schneider, A. Garsuch, A. Panchenko, O. Gronwald, N. Janssen, P. Novák, Influence of different electrode compositions and binder materials on the performance of lithium–sulfur batteries, J. Power Sources. 205 (2012) 420–425. https://doi.org/10.1016/j.jpowsour.2011.12.061.

[4] Z. Deng, Z. Zhang, Y. Lai, J. Liu, J. Li, Y. Liu, Electrochemical Impedance Spectroscopy Study of a Lithium/Sulfur Battery: Modeling and Analysis of Capacity Fading, J. Electrochem. Soc. 160 (2013) A553–A558. https://doi.org/10.1149/2.026304jes.

[5] S. Risse, N.A. Cañas, N. Wagner, E. Härk, M. Ballauff, K.A. Friedrich, Correlation of capacity fading processes and electrochemical impedance spectra in lithium/sulfur cells, J. Power Sources. 323 (2016) 107–114. https://doi.org/10.1016/j.jpowsour.2016.05.032.

[6] J. Fang, W. Shen, S.H.S. Cheng, S. Ghashghaie, H.K. Shahzad, C.Y. Chung, Four-electrode symmetric setup for electrochemical impedance spectroscopy study of Lithium–Sulfur batteries, J. Power Sources. 441 (2019) 227202. https://doi.org/10.1016/j.jpowsour.2019.227202.

[7] N.A. Cañas, K. Hirose, B. Pascucci, N. Wagner, K.A. Friedrich, R. Hiesgen, Investigations of lithium–sulfur batteries using electrochemical impedance spectroscopy, Electrochimica Acta. 97 (2013) 42–51. https://doi.org/10.1016/j.electacta.2013.02.101.

[8] D.N. Fronczek, W.G. Bessler, Insight into lithium–sulfur batteries: Elementary kinetic modeling and impedance simulation, J. Power Sources. 244 (2013) 183–188. https://doi.org/10.1016/j.jpowsour.2013.02.018.

[9] V.S. Kolosnitsyn, E.V. Kuzmina, E.V. Karaseva, S.E. Mochalov, A study of the electrochemical processes in lithium–sulphur cells by impedance spectroscopy, J. Power Sources. 196 (2011) 1478–1482. https://doi.org/10.1016/j.jpowsour.2010.08.105.

[10] S. Waluś, A. Robba, R. Bouchet, C. Barchasz, F. Alloin, Influence of the binder and preparation process on the positive electrode electrochemical response and Li/S system performances, Electrochimica Acta. 210 (2016) 492–501. https://doi.org/10.1016/j.electacta.2016.05.130.

[11] J. Conder, C. Villevieille, S. Trabesinger, P. Novák, L. Gubler, R. Bouchet, Electrochemical impedance spectroscopy of a Li–S battery: Part 1. Influence of the electrode and electrolyte compositions on the impedance of symmetric cells, Electrochimica Acta. 244 (2017) 61–68. https://doi.org/10.1016/j.electacta.2017.05.041.

[12] A. Ganesan, A. Varzi, S. Passerini, M.M. Shaijumon, Graphene derived carbon confined sulfur cathodes for lithium-sulfur batteries: Electrochemical impedance studies, Electrochimica Acta. 214 (2016) 129–138. https://doi.org/10.1016/j.electacta.2016.08.030.

[13] X. Qiu, Q. Hua, L. Zheng, Z. Dai, Study of the discharge/charge process of lithium–sulfur batteries by electrochemical impedance spectroscopy, RSC Adv. 10 (2020) 5283–5293. https://doi.org/10.1039/C9RA10527A.

[14] C. Bünzli, H. Kaiser, P. Novák, Important Aspects for Reliable Electrochemical Impedance Spectroscopy Measurements of Li-Ion Battery Electrodes, J. Electrochem. Soc. 162 (2014) A218. https://doi.org/10.1149/2.1061501jes.

[15] S. Waluś, C. Barchasz, R. Bouchet, J.-F. Martin, J.-C. Leprêtre, F. Alloin, Investigation of non-woven carbon paper as a current collector for sulfur positive electrode—Understanding of the mechanism and potential applications for Li/S batteries, Electrochimica Acta. 211 (2016) 697–703. https://doi.org/10.1016/j.electacta.2016.05.204.

[16] W. Li, H. Yao, K. Yan, G. Zheng, Z. Liang, Y.-M. Chiang, Y. Cui, The synergetic effect of lithium polysulfide and lithium nitrate to prevent lithium dendrite growth, Nat. Commun. 6 (2015) 7436. https://doi.org/10.1038/ncomms8436.

[17] C.-S. Kim, A. Guerfi, P. Hovington, J. Trottier, C. Gagnon, F. Barray, A. Vijh, M. Armand, K. Zaghib, Importance of open pore structures with mechanical integrity in designing the cathode electrode for lithium–sulfur batteries, J. Power Sources. 241 (2013) 554–559. https://doi.org/10.1016/j.jpowsour.2013.05.026.

[18] M. Hagen, G. Feisthammel, P. Fanz, H.T. Grossmann, S. Dörfler, J. Tübke, M.J. Hoffmann, D. Börner, M. Joos, H. Althues, S. Kaskel, Sulfur Cathodes with Carbon Current Collector for Li-S cells, J. Electrochem. Soc. 160 (2013) A996–A1002. https://doi.org/10.1149/2.149306jes.

[19] K.A. Seid, J.-C. Badot, O. Dubrunfaut, S. Levasseur, D. Guyomard, B. Lestriez, Multiscale electronic transport mechanism and true conductivities in amorphous carbon–LiFePO4 nanocomposites, J. Mater. Chem. 22 (2012) 2641–2649. https://doi.org/10.1039/C2JM13429B.

[20] J.Y. Song, H.H. Lee, Y.Y. Wang, C.C. Wan, Two- and three-electrode impedance spectroscopy of lithium-ion batteries, J. Power Sources. 111 (2002) 255–267. https://doi.org/10.1016/S0378-7753(02)00310-5.

[21] N. Schweikert, H. Hahn, S. Indris, Cycling behaviour of Li/Li4Ti5O12 cells studied by electrochemical impedance spectroscopy, Phys. Chem. Chem. Phys. 13 (2011) 6234–6240. https://doi.org/10.1039/C0CP01889A.

[22] S. Drvarič Talian, J. Bobnar, A.R. Sinigoj, I. Humar, M. Gaberšček, Transmission Line Model for Description of the Impedance Response of Li Electrodes with Dendritic Growth, J. Phys. Chem. C. 123 (2019) 27997–28007. https://doi.org/10.1021/acs.jpcc.9b05887.

[23] J.-J. Woo, V.A. Maroni, G. Liu, J.T. Vaughey, D.J. Gosztola, K. Amine, Z. Zhang, Symmetrical Impedance Study on Inactivation Induced Degradation of Lithium Electrodes for Batteries Beyond Lithium-Ion, J. Electrochem. Soc. 161 (2014) A827–A830. https://doi.org/10.1149/2.089405jes.

[24] S.F. Sciamanna, S. Lynn, Sulfur solubility in pure and mixed organic solvents, Ind. Eng. Chem. Res. 27 (1988) 485–491. https://doi.org/10.1021/ie00075a019.

[25] S. Drvarič Talian, J. Bobnar, J. Moškon, R. Dominko, M. Gaberšček, Effect of high concentration of polysulfides on Li stripping and deposition, Electrochimica Acta. 354 (2020) 136696. https://doi.org/10.1016/j.electacta.2020.136696.

[26] V.S. Kolosnitsyn, E.V. Kuzmina, S.E. Mochalov, Determination of lithium sulphur batteries internal resistance by the pulsed method during galvanostatic cycling, J. Power Sources. 252 (2014) 28–34. https://doi.org/10.1016/j.jpowsour.2013.11.099.

[27] S. Waluś, C. Barchasz, R. Bouchet, J.-C. Leprêtre, J.-F. Colin, J.-F. Martin, E. Elkaïm, C. Baehtz, F. Alloin, Lithium/Sulfur Batteries Upon Cycling: Structural Modifications and Species Quantification by In Situ and Operando X-Ray Diffraction Spectroscopy, Adv. Energy Mater. 5 (2015) 1500165. https://doi.org/10.1002/aenm.201500165.

[28] S. Waluś, C. Barchasz, J.-F. Colin, J.-F. Martin, E. Elkaïm, J.-C. Leprêtre, F. Alloin, New insight into the working mechanism of lithium–sulfur batteries: in situ and operando X-ray diffraction characterization, Chem. Commun. 49 (2013) 7899–7901. https://doi.org/10.1039/C3CC43766C.

[29] S. Drvarič Talian, J. Moškon, R. Dominko, M. Gaberšček, Impedance response of porous carbon cathodes in polysulfide redox system, Electrochimica Acta. 302 (2019) 169–179. https://doi.org/10.1016/j.electacta.2019.02.037.

[30] S. Devan, V.R. Subramanian, R.E. White, Analytical Solution for the Impedance of a Porous Electrode, J. Electrochem. Soc. 151 (2004) A905. https://doi.org/10.1149/1.1739218.

[31] J. Huang, J. Zhang, Theory of Impedance Response of Porous Electrodes: Simplifications, Inhomogeneities, Non-Stationarities and Applications, J. Electrochem. Soc. 163 (2016) A1983. https://doi.org/10.1149/2.0901609jes.

[32] J.Y. Song, H.H. Lee, Y.Y. Wang, C.C. Wan, Two- and three-electrode impedance spectroscopy of lithium-ion batteries, J. Power Sources. 111 (2002) 255–267. https://doi.org/10.1016/S0378-7753(02)00310-5.

Figure caption

Figure 1: Characteristic Nyquist plot of a fresh Li/S coin cell at the initial state measured at 25°C..

Figure 2: Comparison of the Nyquist plots obtained for fresh Li/S (black), symmetric Li||Li (red) and $S_8||S_8$ (blue) cells (a). Overlay of the calculated Nyquist plot ($Z_{Li-S} = ½ Z_{Li-Li} + ½ Z_{S-S}$) using the data of the symmetric cells and the experimental one (b).

Figure 3: Li/S cells was left for 250h aging in open circuit condition at 25°C, EIS was recorded every 30 min. OCV evolution of the Li/S cell (a), Nyquist plot evolution observed during initial few hours of aging of the Li/S cell (b), and after further hours of storage (c). As a matter of comparison, evolution of the Nyquist plots of a symmetric Li/Li cell aging in the same conditions (d).

Figure 4: Nyquist plots evolution during the first discharge and charge. Numbers in red along the charge/discharge curves in the inset indicate the points where EIS was recorded.

Figure 5: Equivalent electrical circuit used for fitting all the *in situ* EIS data, and physico-chemicals processes associated with each circuit component. An example of fit of the experimental spectra is given using a spectrum obtained at 80% DOD.

Figure 6: Evolution of the different resistance values, R_{el}, R_{Li}, R_{NwC} and $R_{PS,}$ extracted from the spectra Figure 4, as a function of SoC% during the first discharge and charge.

Figure 7: Discharge capacity retention during 7 cycles (black circles) together with the maximum value of the electrolyte resistance evolution (red diamonds), recorded at every discharge.

Figure 8: Voltage profiles of Li/S cell obtained at a low rate of C/100 and at different temperatures, decreasing from 0°C to -40°C.

Figure 9: Electrolyte resistance evolution along the first discharge and charge cycle recorded at different temperatures: 25°C, 0°C, -20°C and -30°C (a). Evolution of the maximum resistance values *vs* temperature in Arrhenius plot (b).

Figure 10: Nyquist plots recorded at the end of the discharge (a) and the charge (b) at different temperatures: 25°C, 0°C, -20°C and -30°C.

Figures

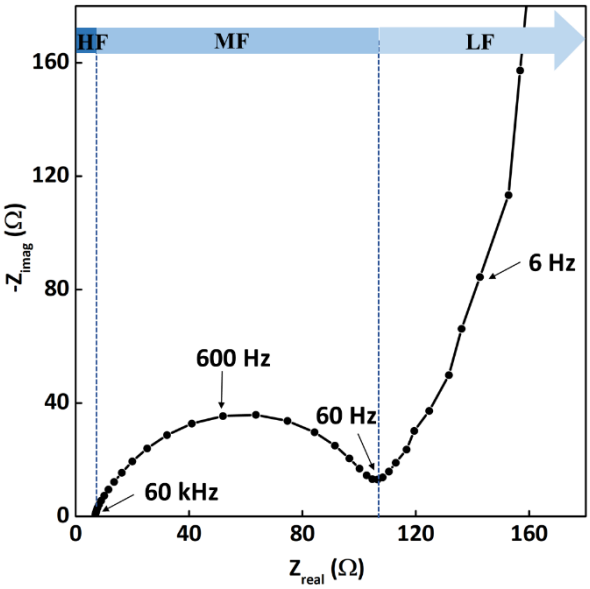

Figure 1

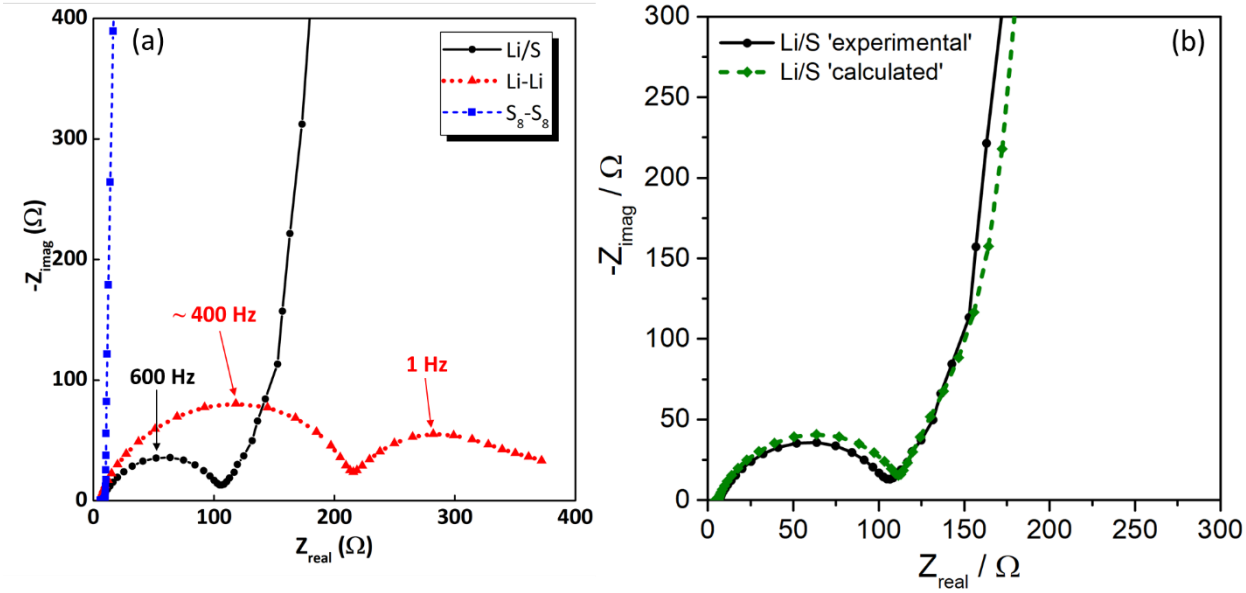

Figure 2

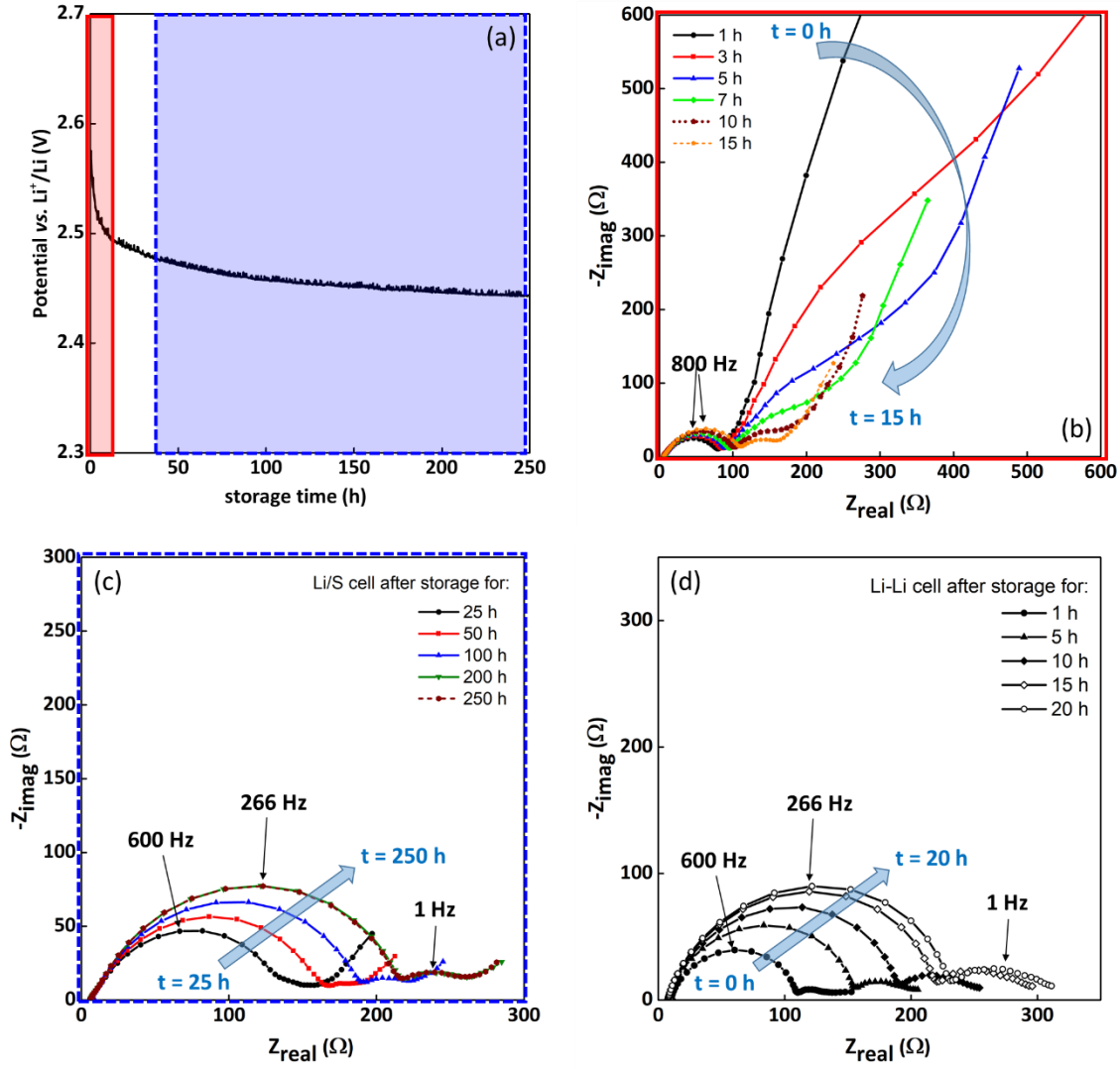
(a)
Potential vs. Li+/Li (V)
storage time (h)
(b)
1 h
3 h
5 h
7 h
10 h
15 h
t = 0 h
800 Hz
t = 15 h
-Zimag (Ω)
Zreal (Ω)
(c)
Li/S cell after storage for:
25 h
50 h
100 h
200 h
250 h
600 Hz
266 Hz
t = 250 h
1 Hz
t = 25 h
-Zimag (Ω)
Zreal (Ω)
(d)
Li-Li cell after storage for:
1 h
5 h
10 h
15 h
20 h
600 Hz
266 Hz
t = 20 h
1 Hz
t = 0 h
-Zimag (Ω)
Zreal (Ω)

Figure 3

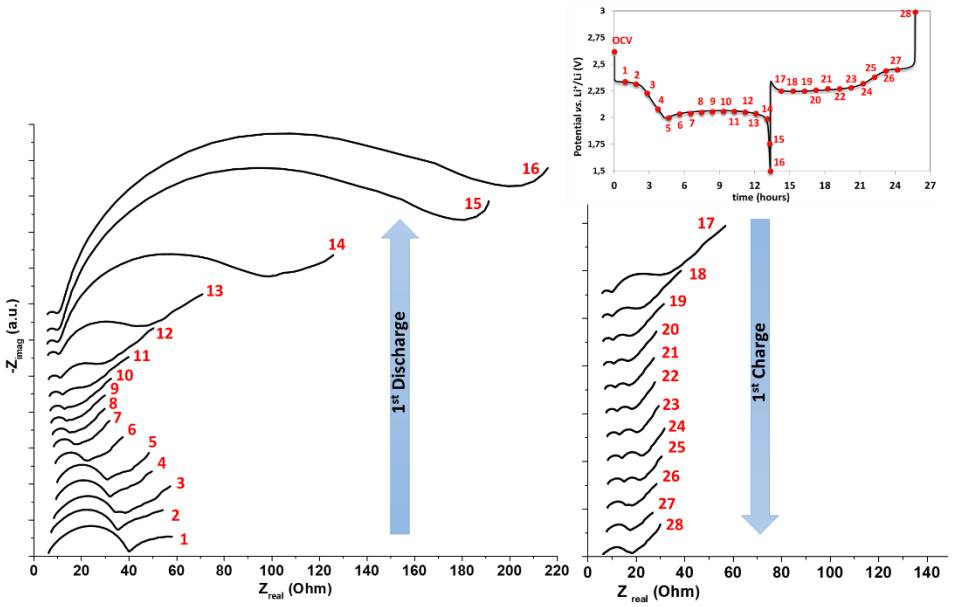

Figure 4

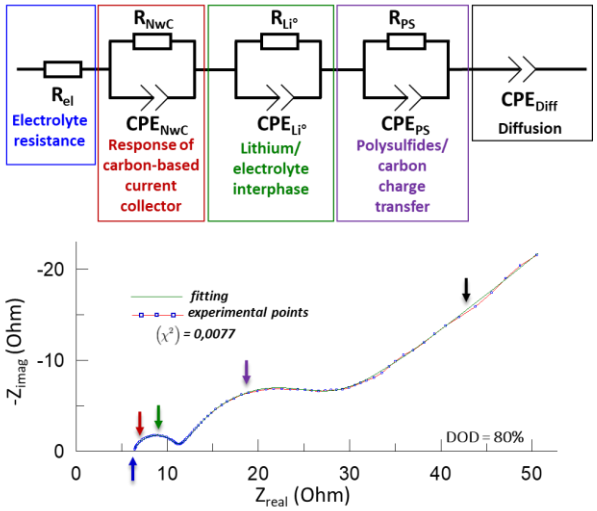

Figure 5

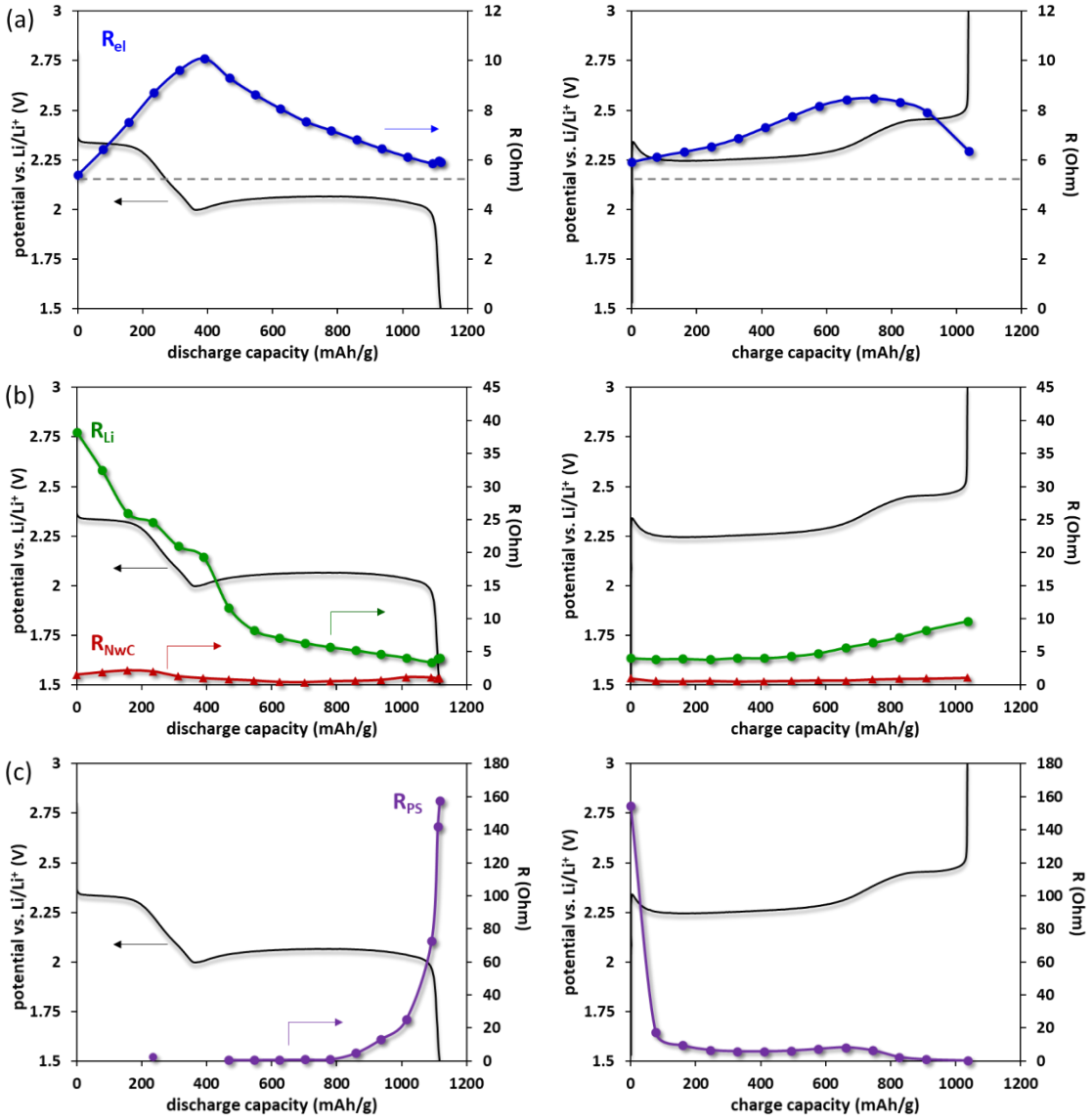
(a)
R_{el}
potential vs. Li/Li+ (V)
R (Ohm)
discharge capacity (mAh/g)
charge capacity (mAh/g)
(b)
R_{Li}
R_{NwC}
(c)
R_{PS}

Figure 6

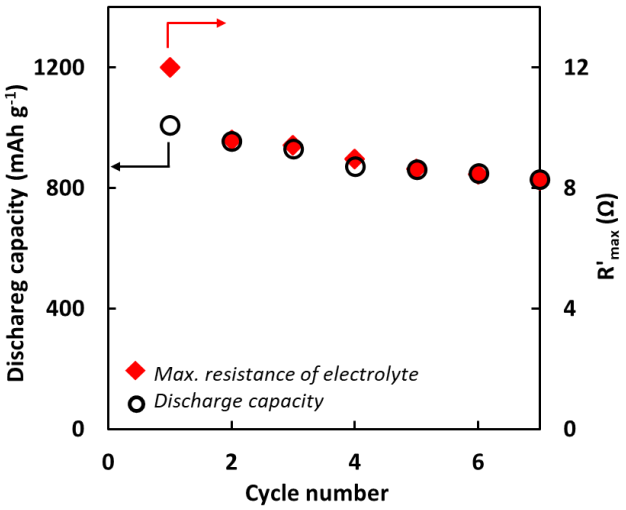

Figure 7

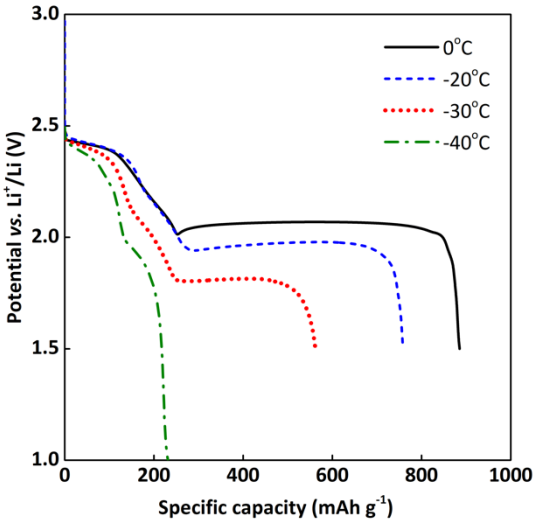

Figure 8

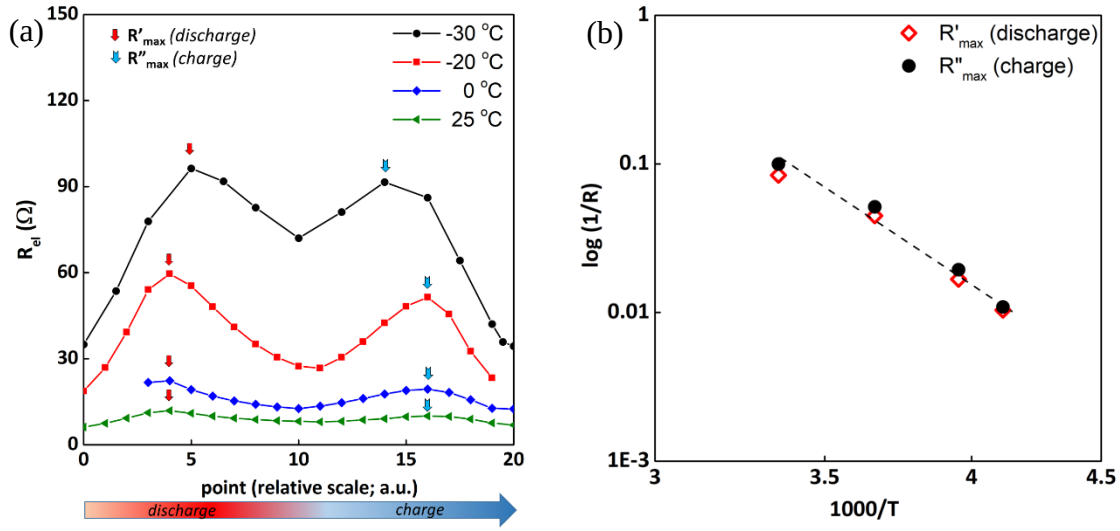

Figure 9

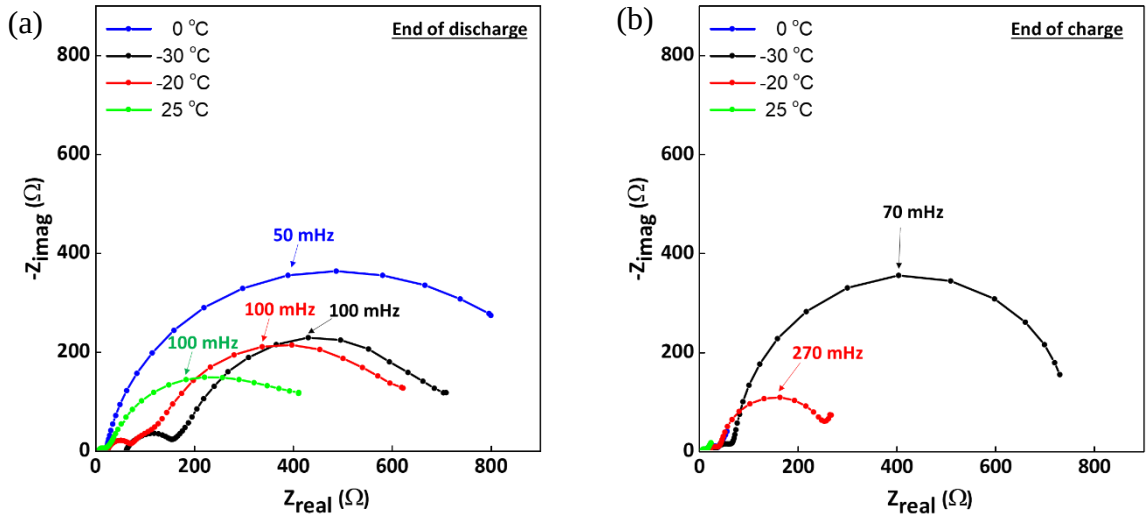

Figure 10